# 3D RECONSTRUCTION OF 2D CRYSTALS FROM PROJECTIONS IN REAL SPACE

*Roberto Marabini, Gabor T. Herman* [*]
The Graduate Center
The City University of New York
New York, NY 10016, USA

*José J. Fernández* [†]
Dept. Arquitec. de Comp. y Electrónica
U. Almería, 04120 Almería, Spain

*Carlos O. S. Sorzano, José M. Carazo* [‡]
Centro Nacional de Biotecnología-CSIC
Campus Universidad Autónoma de Madrid
28049 Madrid, Spain

*Samuel Matej*
Blockley Hall 4th Fl.
University of Pennsylvania
Philadelphia, PA 19104, USA

## ABSTRACT

A new algorithm for 3D reconstruction of two-dimensional crystals from projections is presented, and applied to biological macromolecules imaged using electron microscopy. Its main departure from the traditional approach is that it works in real space, rather than in Fourier space, and is iterative. This approach has the advantage of making it convenient to introduce additional constraints (such as the support of the function to be reconstructed, which may be known from alternative measurements) and has the potential of more accurately modeling the electron microscope image formation process.

## 1. INTRODUCTION

The analysis by transmission electron microscopy (TEM) of biological material is inconvenienced by its sensitivity to electron radiation. In order to minimize the damage caused by the radiation, the electron dose is kept low and consequently the signal to noise ratio of the images is poor.

Image processing methods have been developed to counter this problem. Although, ideally, these methods can be applied to a TEM image of any object, they are usually most powerful for objects in which subunits are arranged in a regular manner, such as two-dimensional biological crystals. When processing images of such periodic objects, Fourier transformation is usually employed [1]. This is due to the fact that their Fourier transform (FT) is zero valued except at isolated points. This property often enables a convenient manipulation of the data. 2D crystals are currently the only way to reach atomic resolution using electron microscopy [2, 3]

In this work an iterative method for performing three-dimensional reconstruction of 2D crystals in real space is proposed. We see two potential advantages of this approach over the traditional methods in the Fourier space. First, it avoids interpolations in Fourier domain that often generate artifacts (especially when the number of projections is small). Second, it allows the convenient incorporation of information available from other microscopies [4, 5] and from adequate modeling either of the sample [6] or of the imaging device [7].

## 2. THEORETICAL BACKGROUND

### 2.1. Outline of the Fourier space method of crystal reconstruction

The 3D reconstruction process starts by obtaining a number of projections of the object at different angles and calculating their Fourier transforms. In the case of crystalline specimens (that is, specimens made by regular repetitions of a *motif* or *unit cell*) the crystal projections can be described as the convolution of a *bidimensional Shah* [1] function (usually called *the real lattice*) and a 2D motif. The FT of a Shah function is another Shah function (usually called *the reciprocal lattice*). Therefore, the projection FT will be the product of a Shah function and the FT of the 2D motif. Even with imperfect real specimens the structural information in the FT is concentrated at the points of the reciprocal lattice usually called *reflections* or *spots*. Once we have the FTs of all the projection images, the next step is to calculate the

[*] Partially supported by NIH grant HL70472.
[†] Partially supported by grant TIC99-0361.
[‡] Partially supported by grants BIO98-0761, BIO2001-1237 and TIC990361 from the "Comisión Interministerial de Ciencia y Tecnología" of Spain

[1] A simple example of a bidimensional Shah function is: $^2\mathrm{III} = \sum_{m=-\infty}^{\infty}\sum_{n=-\infty}^{\infty}\delta(x-m)\delta(y-n)$.

specimen 3D FT by applying the *central section theorem.* [2] As we are working with crystals that repeat themselves only in two dimensions, the crystal 3D FT is not a collection of spots, but is a collection of lines parallel to the $Z^*$ axis (that is, perpendicular to the crystal plane). These lines are called *lattice lines* and their intersection with the central sections are the spots whose values are given by the projection FTs. If the number of different projections is high enough, the specimen 3D FT (that is, the lattice lines) can be recovered.

The traditional approach combines the projections in Fourier space to obtain a non-uniformly sampled 3D FT. From this a uniformly sampled 3D FT is calculated by 1D interpolation along the lattice lines. The interpolation is made by a least squares algorithm [8]. It is recommended that experimental data be obtained at a third or fourth of the desired sampling rate in Fourier space, which is the inverse of the specimen thickness.

### 2.2. Outline of the *Algebraic Reconstruction Techniques* (ART) used as base of our novel reconstruction algorithm for 2D crystals

Algebraic reconstruction techniques are series expansion methods [9]; i.e., they assume that a volume $v$ can be approximated by a linear combination of a finite set of known basis functions $b_j$ centered at $J$ grid points as in

$$v(\mathbf{r}) \approx \sum_{j=0}^{J-1} x_j b_j(\mathbf{r}) \tag{1}$$

and the task of the algorithm is to estimate the unknown coefficients $x_j$ (for a review on ART, see [10]). A consequence of Eq. 1 is an image formation model of the form:

$$y_i = \sum_{j=0}^{J-1} l_{i,j} x_j \tag{2}$$

where $y_i$ is the $i$th measurement of the volume to be reconstructed (that is, a pixel of the experimental data) and $l_{i,j}$ is the corresponding line integral of the basis function $b_j$. The values $y_i$ and $x_j$ form a $MN$-dimensional vector and a $J$-dimensional vector that we will name $\mathbf{y}$ and $\mathbf{x}$ respectively, where $M$ is the number of projections and $N$ the number of pixels per projection.

The particular variant of ART that we use as the basis of our algorithm operates as follows. Starting with a $J$-dimensional zero vector for the estimate of $\mathbf{x}$, we update this estimate of $\mathbf{x}$ iteratively. In an iterative step we made use of data from one projection only; we repeatedly cycle though all the projections in the complete algorithm. The update of the estimate of $\mathbf{x}$ is done in a computationally efficient manner so as to reduce the discrepancy between the measured data provided by the projection used in that iterative step and the matching *pseudo projection data* that is obtained from the current estimate of $x$ using the right hand side of Eq. 2. Following Lewitt [11] we use spherically symmetric basis functions. The arrangement of the centers of these functions is referred to as the *grid*. The choice of the grid influences the quality of the reconstruction. It was found that grids different from the cubic one are preferable, in particular the use of the so-called body-centered cubic grid (BCC) is recommended [12].

[2] The central section theorem states that the FT of any projection $p$ of a volume $v$ is equal to one plane through the origin of the FT of $v$. This plane is often referred to as *the central section*.

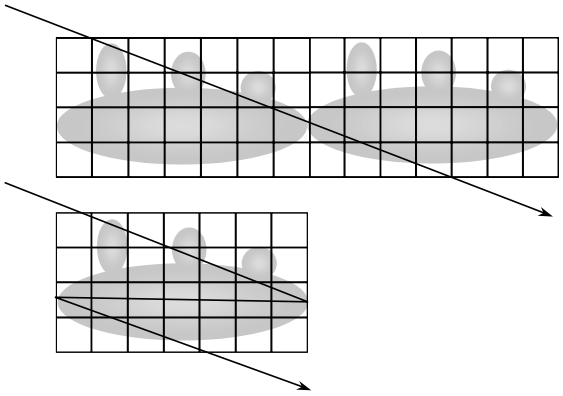

**Fig. 1**: ART may be adapted to reconstruction of 2D crystals by redefining the notion of *line of integration*. The upper part of the image shows a projection beam crossing two unit cells. The lower part of the image shows an equivalent trajectory using a single unit cell.

## 3. ART FOR CRYSTALS

The new reconstruction algorithm takes advantage of the crystal periodicity and only keeps in memory a single copy of these unit cells. Certainly, the projection lines may go through several unit cells, but this difficulty is easily overcome by redefining the projection lines as shown in Fig. 1.

Using a single unit cell of the volume also forces us to modify the choice of the grid. The BCC grid has desirable properties (uniform sampling of the space, symmetries, etc), these are lost if we simply choose our grid for a unit cell to be those points of the BCC grid which happened to fall in the unit cell. Similarly, it is desirable to estimate projection data points which uniformly cover the unit cell in the projections.

Thus, in developing this new algorithm particular attention have had to be payed to the following points: which grids should be used, how a volume approximated as in Eq. 1 using a given grid is related to its projections sampled on different grids and how crystallographic symmetry is implemented. Space constraints preclude a detailed and

mathematical description of the algorithm. Nevertheless, before going to the results section we note that the approach taken is conceptually similar to the one named *squashing* [11, 13] in which given two volumes $v_1$ and $v_2$ related by a linear transformation (that is, one is a *deformed* or *squashed* version of the other); the goal is to reconstruct the volume $v_1$ from data measured using the volume $v_2$.

### 3.1. Results

Various tests have been performed with mathematical phantoms. The results show (see Figs. 2, 3 and 4) that if the number of projection images is low, then the reconstruction obtained with the new algorithm is superior to that of the traditional algorithm.

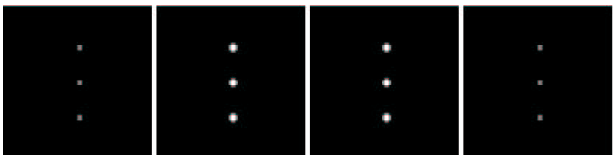

**Fig. 2**: Central slices of a $64 \times 64 \times 64$ voxels phantom composed of three small spheres (radius = 1.75 voxel edge). The density of the voxel $v_i$ is proportional to the volume of the voxel intersection with the small spheres (being equal to one when it is totally inside one of them). The image shows the planes perpendicular to the Y axis (the tilt axis is parallel to the Y axis).

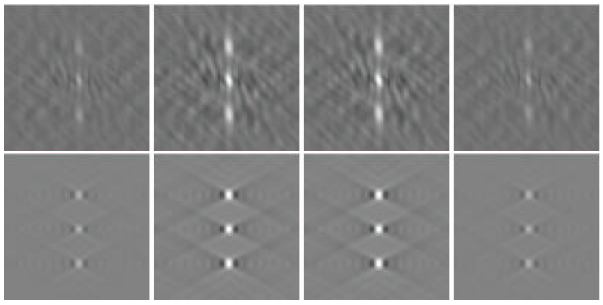

**Fig. 3**: Central slices (matching those in Fig. 2) of 3D reconstructions obtained using the traditional algorithm. The reconstructions in the upper and lower rows have been obtained from 13 and 49 noiseless projections respectively. The gamma of the images has been slightly increased so that differences in the background are more noticeable.

The theoretical explanation of this is based on the interpolation in Fourier space carried out by the classical algorithm: if the number of samples is small the interpolation is poor. An example will clarify the situation: the first

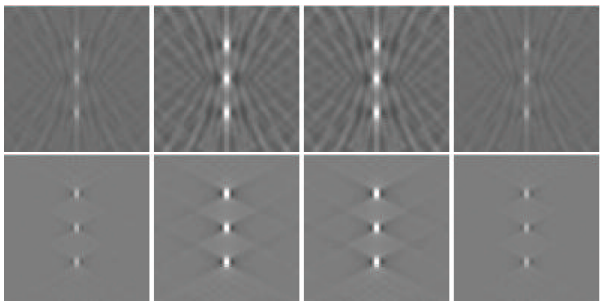

**Fig. 4**: Central slices (matching those in Fig. 2) of 3D reconstructions obtained using the new ART based algorithm. The reconstructions in the upper and lower rows have been obtained from 13 and 49 noiseless projections respectively. The gamma of the image has been adjusted in the same way as in Fig. 3.

phantom is formed by three small spheres that can be approximated by very pointy Gaussians. Therefore, the magnitude of their Fourier transforms should look like a very flat Gaussian (as the traditional method reduces the 3D reconstruction to a set of 1D problems -each one of the lattice lines (see 2.1) is calculated independently- in the following we will assume that the Gaussians are 1D). If a pointy Gaussian is near to the origin, then the phase of its FT is (nearly) constant; therefore, we have a function that is very easy to interpolate. As it is moved farther away from the origin the faster is the change in the phase of its FT and the more difficult is the interpolation. On the other hand, ART solves almost the same system of equations regardless of the spatial localization of the spheres.

In our tests with phantoms, and when the number of projections is high enough, the traditional method produces reconstructions similar to the new method. Currently more realistic phantoms, like the one shown in Fig. 5, are being designed to accurately compare the two reconstruction algorithms. In these new phantoms the projections are calculated from the protein atomic coordinates.

### 3.2. Future Work

Our main motivation for implementing a reconstruction algorithm for crystals that works in real space and is iterative is not to replace the well established methods used at present but to create a framework in which we can easily incorporate information available from other sources. This information, such as surface reliefs from atomic or shadowing microscopies (see [15, 16] for a description of our work in this area), or a more suitable model of the imaging device (contrast transfer function; see [16]) is more easily and naturally incorporated in a real space iterative method than in a Fourier space based algorithm. For example, in the ART

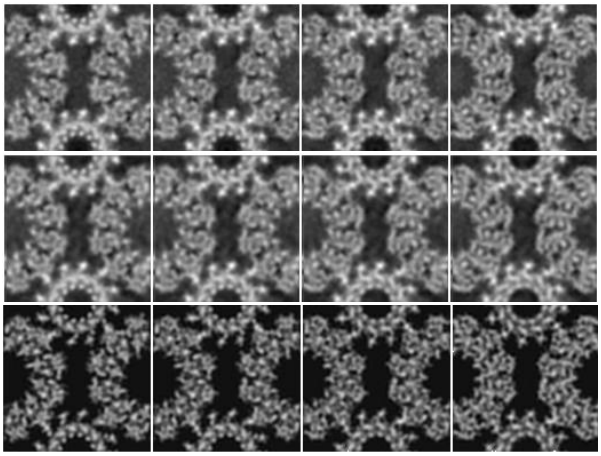

**Fig. 5**: Reconstruction of a phantom of the bacteriophage $\phi 29$ connector using the traditional algorithm (top) and the new algorithm (middle). Low-pass filtered version of a density volume of the same structure created from atomic coordinates [14] (botton).

based method, the contrast transfer function can be taken into account by modifying the $l_{i,j}$ in the system matrix (see Eq. 2) without any modification of the algorithm's logic.

## 4. REFERENCES


[1] R. Henderson, J. M. Baldwin, K. H. Downing, J. Lepault, and F. Zemlin, "Structure of purple membrane from *Halobacterium halobium:* recording, measurement and evaluation of electron micrographs at 3.5 Å resolution," *Ultramicroscopy*, vol. 19, pp. 147–178, 1986.

[2] R. Henderson, J. M. Baldwin, T. A. Ceska, F. Zemlin, E. Beckmann, and K. H. Downing, "Model for the structure of bacteriorhodopsin based on high-resolution electron cryo-microscopy," *J. Mol. Biol.*, vol. 213, pp. 899–929, 1990.

[3] W. Khlbrandt, D. N. Wang, and Y. Fujiyoshi, "Atomic model of plant light-harvesting complex by electron crystallography," *Nature*, vol. 367, pp. 614–621, 1994.

[4] P. R. Smith and J. Kistler, "Surface reliefs computed from micrographs of isolated heavy metal shadowed particles.," *J. Ultrastruc. Res.*, vol. 71, pp. 25–36, 1980.

[5] D. J. Müller, A. Engel, J. L. Carrascosa, and M. Vélez, "The bacteriophage $\phi 29$ head-tail connector imaged at high resolution with the atomic force microscope in buffer solution," *EMBO Journal*, vol. 16, pp. 2547–2553, 1997.

[6] M.T. Chan, G.T. Herman, and E. Levitan, "Bayesian image reconstruction using image-modeling Gibbs priors," *Int. J. Imag. Syst. Tech.*, vol. 9, pp. 85–98, 1998.

[7] L. A. Amos, R. Henderson, and P. N. T. Unwin, "Three-dimensional structure determination by electron microscopy of two-dimensional crystals," *Prog. Biophys. Mol. Biol.*, vol. 39, pp. 183–231, 1982.

[8] D. A. Agard, "A least-squares method for determining structure factors in three-dimensional tilted-view reconstructions.," *J. Mol. Biol.*, vol. 167, no. 4, pp. 849–52, 1983.

[9] G.T. Herman, *Image Reconstruction from Projections: The Fundamentals of Computerized Tomography*, Academic Press, New York, 1980.

[10] G.T. Herman, "Algebraic reconstruction techniques in medical imaging," in *Medical Imaging, Systems Techniques and Applications*, C.T. Leondes, Ed., vol. 6: Computational Techniques, pp. 1–42. Gordon and Breach Science Publishers, Amsterdam, 1998.

[11] R.M. Lewitt, "Alternatives to voxels for image representation in iterative reconstruction algorithms," *Phys. Med. Biol.*, vol. 37, pp. 705–716, 1992.

[12] S. Matej and R. M. Lewitt, "Efficient 3D grids for image reconstruction using spherically-symmetric volume elements," *IEEE Trans. Nucl. Sci.*, vol. 42, pp. 1361–1370, 1995.

[13] J. A. Reeds and L. A. Shepp, "Limited Angle Reconstruction in Tomography via Squashing," *IEEE Trans. Med. Imag.*, vol. 6, pp. 89–97, 1987.

[14] A. A. Simpson, Y. Z. Tao, P. G. Leiman, M. O. Badasso, Y. N. He, P. J. Jardine, N. H. Olson, M. C. Morais, S. Grimes, D. L. Anderson, T. S. Baker, and M. G. Rossmann, "Structure of the bacteriophage phi 29 DNA packaging motor," *Nature*, vol. 408, pp. 745–750, 2000.

[15] E. Dimmeler, R. Marabini, P. Tittmann, and H. Gross, "Correlation of topographic surface and volume data from 3D electron microscopy.," *J. Struc. Biol.*, 2002, in press.

[16] G. T. Herman, R. Marabini, J. M. Carazo, E. Garduño, R.M. Lewitt, and S. Matej, "Image processing approaches to biological three-dimensional electron microscopy," *Int. J. Imag. Syst. Tech.*, vol. 11, pp. 12–29, 2000.